The insect nephrocyte is a podocyte-like cell with a filtration slit diaphragm

Helen Weavers[1*], Silvia Prieto-Sánchez[2*], Ferdinand Grawe[3], Amparo Garcia-López[4], Ruben Artero[4], Michaela Wilsch-Braeuninger[5], Mar Ruiz-Gómez[2], Helen Skaer[1] and Barry Denholm[1]

1. Department of Zoology, University of Cambridge, Downing Street, Cambridge, CB2 3EJ, UK

2. Centro de Biología Molecular Severo Ochoa, CSIC, UAM, Cantoblanco, 28049, Madrid, Spain.

3. Institut für Genetik, Heinrich-Heine-Universität, Düsseldorf, D-40225, Germany

4. Department of Genetics, University of Valencia, Burjasot, Valencia 46100, Spain

5. Max Planck Institute of Molecular Cell Biology and Genetics, Dresden, Germany

** these authors contributed equally to this work*

Author for correspondence: hs17@cam.ac.uk

The nephron is the basic structural and functional unit of the vertebrate kidney. It is composed of a glomerulus, the site of ultrafiltration, and a renal tubule, along which the filtrate is modified. Although widely regarded as a vertebrate adaptation[1] 'nephron-like' features can be found in the excretory systems of many invertebrates, raising the possibility that components of the vertebrate excretory system were inherited from their invertebrate ancestors[2]. Here we show that the insect nephrocyte has remarkable anatomical, molecular and functional similarity with the glomerular podocyte, a cell in the vertebrate kidney that forms the main size-selective barrier as blood is ultrafiltered to make urine. In particular, both cell types possess a specialised filtration diaphragm, known as the slit diaphragm in podocytes or the nephrocyte diaphragm in nephrocytes. We find that fly orthologues of the major constituents of the slit diaphragm, including nephrin, neph1, CD2AP, ZO-1 and podocin are expressed in the nephrocyte and form a complex of interacting proteins that closely mirrors the vertebrate slit diaphragm complex. Furthermore, we find the nephrocyte diaphragm is completely lost in flies mutant for nephrin or neph1 orthologues, a phenotype resembling loss of the slit diaphragm in the absence of either nephrin (as in the human kidney disease NPHS1) or neph1. These changes drastically impair filtration function in the nephrocyte. The similarities we describe between invertebrate nephrocytes and vertebrate podocytes provide evidence suggesting the two cell types are evolutionarily related and establish the nephrocyte

as a simple model in which to study podocyte biology and podocyte-associated diseases.

Filtration of blood in the vertebrate kidney occurs within the glomerulus of the nephron. Here, fluid is forced by blood pressure across a filtration barrier producing a primary urine free from cells and large proteins, which is then modified as it passes along the renal tubule, before being excreted (Fig. 1a). The glomerular filtration barrier is formed in part from highly specialised epithelial cells known as podocytes. These cells send out numerous foot processes that interdigitate with those of adjacent podocytes, forming a layer that completely enwraps the glomerular capillaries. The foot processes are separated by 30-50nm wide slit pores, spanned by a filtration diaphragm, the slit diaphragm[3,4]. Together, the slit diaphragm and the glomerular basement membrane (GBM) form a size- and charge-selective filtration barrier (Fig. 1b). Disruption to this barrier in diseases that perturb the structure of the slit diaphragm or GBM lead to leakage of blood proteins into the urinary space and, frequently, to kidney failure[5].

Although the excretory systems of invertebrates are considered to lack nephrons, 'nephron-like' components, such as filtration cells and ducts in which the filtrate is modified, are widespread. These include protonephridia in planaria, podocytes and pore cells in gastropod molluscs, antennal glands in crustaceans, and Malpighian tubules and nephrocytes of insects (Fig. 1c)[6,7]. Nephrocytes regulate haemolymph composition by filtration, followed by endocytosis and processing of the filtrate to sequester and/or secondarily metabolise toxic materials[7-9]. *Drosophila* has two types – garland (Fig. 1e,g)

and pericardial (Fig. 1f) nephrocytes. They are tethered to the oesophagus (Fig. 1g and 3g) or to the heart and associated muscles (Fig. 1f), and are bathed in haemolymph. Extensive infolding of the plasma membrane generates a network of labyrinthine channels or lacunae flanked by nephrocyte foot processes (Fig. 1h). The channel entrances are narrow slits 30nm in width, spanned by a specialised filtration junction known as the nephrocyte diaphragm – a single or double filament extending between adjacent foot processes (Fig. 1h,i and Fig. 3c). Each nephrocyte is enveloped by basement membrane (Fig. 1h and Fig. 3c). Together, the nephrocyte diaphragm and basement membrane behave as a size and charge-selective barrier[7,9] (Fig. 1d) and filtrate is endocytosed from the sides of the lacunae. Thus the anatomy of the nephrocyte filtration barrier is remarkably similar to that of the glomerular filtration barrier[3].

In view of this similarity we investigated whether the nephrocyte diaphragm is molecularly related to the slit diaphragm. The major slit diaphragm components, the transmembrane Ig-domain superfamily proteins nephrin and neph1 ('Ig-domain proteins') are co-expressed in the podocyte and interact across the slit pore by homo- and hetero-typic binding to form the diaphragm[4,10-16]. Mutations in nephrin, as in human congenital nephrotic syndrome of the Finnish type (NPHS1)[10], or in neph1[17], cause slit diaphragm loss and foot process effacement, resulting in break down of the filtration barrier and proteinuria.

Drosophila has two nephrin orthologues – *sticks and stones* (*sns*) and *hibris* (*hbs*) and two neph1 orthologues – *dumbfounded (duf*) and *roughest* (*rst*) (Supplementary Table 1).

As *hbs* and *rst* are expressed in only a subset of nephrocytes (data not shown), we focus on *sns* and *duf*. Sns and Duf are expressed throughout the lifetime of the animal in both nephrocyte cell types (Figs. 2a-g, adult data not shown), from mid embryogenesis (stage 11) for garland cells (Supplementary Fig.1 and Fig. 2a,b) and from the first larval instar for pericardial cells (Fig. 2c). Interestingly, the onset of Sns and Duf expression correlates in time with the appearance of the nephrocyte diaphragm at the ultrastructural level: mid embryogenesis for garland nephrocytes[18] and early first instar for pericardial nephrocytes[19]. Both proteins localise to the plasma membrane (Fig. 2d-g) and double labelling reveals precise co-localisation (Fig. 2h). This finding is initially surprising because in most other contexts Sns and Duf are expressed in complementary patterns and mediate interaction between cells of different type. The only other situation where the two types of Ig-domain proteins are co-expressed and interact in the same cell is the vertebrate podocyte[14]. We find that Sns and Duf are dependent on one another for their mutual stabilization at the plasma membrane. The loss or knock down of one protein in embryonic (Fig 2i-l or larval (Fig 2m-p) nephrocytes leads to a loss, severe reduction or mislocalisation of the other. These data demonstrate an essential interaction between the two proteins in the same cell, similar to those between nephrin and neph1 in the podocyte[13-16]. The precise subcellular location of the proteins was revealed by immuno-electron microscopy. Both Sns and Duf specifically localise to the nephrocyte diaphragm (Fig 2q-s). Double labelling reveals a close colocalisation between the two proteins (Fig. 2t). Furthermore, grazing sections along the length of the diaphragm reveal an alternating pattern of Sns and Duf (Fig. 2u), demonstrating that both proteins are present around the diaphragm.

We find that both garland and pericardial nephrocytes are correctly specified in Sns and Duf mutants (Supplementary Fig. 2a-k). However, given the importance of the Ig-domain proteins in slit diaphragm formation, we used electron microscopy to determine whether the nephrocyte diaphragm is altered in *sns* and *duf* mutants. In wild-type garland cells, nephrocyte diaphragms and associated lacunae appear during embryogenesis (stage 14, Supplementary Fig. 2l), becoming more numerous by the end of embryogenesis (Fig. 1h). Diaphragms densely populate the cell periphery in third instar larvae (Fig. 3c). Strikingly, *sns* or *duf* mutant garland cells completely lack nephrocyte diaphragms at every stage and in most cases we were unable to detect any membrane infoldings or lacunae (cf Fig. 3a,b with Fig.1i, Fig 3c with d, Supplementary Fig. 2m,n with l). Occasional lacunae do form, but are never bridged by diaphragms (Fig. 3b, Supplementary Fig. 2n). Instead, the surface of the nephrocyte undulates and contains frequent, small patches of electron dense subcortical material (Fig. 3a[i]) that could be remnants of undercoat normally associated with the cytoplasmic face of the wild-type diaphragm. These observations suggest that membrane invaginations can occur but that in the absence of the diaphragm, foot processes are unstable and undergo effacement. Scanning electron microscopy reveals the extent of surface smoothening that results from loss of lacunae in mutant garland cells (cf Fig. 3e and f). These phenotypes are remarkably similar to those of podocytes lacking nephrin or neph1[5,17]. Thus, by analogy with nephrin and neph1 in the slit diaphragm, we suggest that the extracellular domains of Sns and Duf interact across the slit pore to form the nephrocyte diaphragm itself.

In addition, we noted that the basement membrane in *sns* knockdown and *duf* larval nephrocytes was irregular and dramatically expanded (cf Fig. 3c,d). The basement membrane in *duf* nephrocytes has an average depth of 202nm (± 24, n=13) compared with 57nm (± 4, n=11) for wild-type nephrocytes. This results from an increase in deposition of the *Drosophila* collagen IV (Viking) (Fig. 3g,h, Supplementary Fig. 3). However this is unlikely to account fully for the four-fold thickening observed, and we suggest that a further contributing factor is the accumulation of haemolymph proteins that clog the basement membrane due to inefficient filtration.

Given the similarities between the morphology and molecular requirements for podocyte and nephrocyte diaphragms, we tested the ability of human nephrin to rescue the *sns* mutant phenotype. However nephrocytes are sensitive to absolute levels of *sns*, so that even moderate overexpression produced abnormal phenotypes. We therefore compared the effects of overexpressing *Drosophila sns* with human nephrin. Their effects are strikingly similar, including abnormal nephrocyte foot process morphology and marked thickening of diaphragm filaments, which span the intercellular space wherever the cytoplasmic coat is thickened (Fig. 3i,j). These data indicate that precise level of Sns is critical for diaphragm formation and more importantly that human nephrin and *Drosophila* Sns function in equivalent ways.

Vertebrate nephrin and neph1 associate with other proteins to form a multi-protein complex at the slit diaphragm (Supplementary Table 1). These include zonula occludens-1 (ZO-1)[20], CD2AP[21,22] and podocin[23]. Mutations in CD2AP result in diaphragm loss and

podocyte foot process effacement in mice[21] and are associated with focal glomerulosclerosis in humans[24]. Mutations in NPHS2, the gene encoding podocin, are associated with sporadic and inherited nephrotic syndromes[23]. We asked whether orthologues of these genes in the fly (Supplementary Table 1) contribute to the nephrocyte junction. *in situ* hybridisation reveals that *pyd* (ZO-1), *CG31012* (CD2AP) and *Mec2* (Supplementary Fig. 4) are expressed in garland (Fig. 4a,c,e) and pericardial (Fig. 4b,d,f) nephrocytes. Furthermore, a Pyd-GFP fusion protein precisely co-localises with Duf to the nephrocyte membrane (Fig. 4g), mirroring co-localisation of ZO-1 and neph1 in the podocyte[20].

Molecular interactions between these vertebrate slit diaphragm-associated proteins have been established (Fig. 4h, black arrows)[11,20,22,25]. To test whether fly orthologues form a similar complex, we performed a yeast two-hybrid analysis with the intracellular domains of Sns and Duf (Fig. 4i). Sns interacts with Mec-2 (NPHS2/podocin) and Duf interacts with Pyd (ZO-1) (Fig. 4j). Interaction between Duf and Pyd was independently confirmed in co-immunoprecipitaion experiments (Fig. 4k). A previous report established direct association between Sns and Duf[26]. These interactions between the fly proteins (Fig. 4h, red arrows) closely resemble those described for slit diaphragm-associated proteins (Fig. 4h, black arrows). These data, taken together with those described above, provide strong evidence that the nephrocyte diaphragm (Fig. 4l) and slit diaphragm are molecularly homologous structures.

Previous studies have shown that insect nephrocytes are selective in their sequestration of materials from the haemolymph and that this selectivity is based on size and charge due to the characteristics of the nephrocyte diaphragm and basement membrane, which act together as a filtration barrier[7,9]. To test filtration capacity of the *Drosophila* nephrocyte diaphragm we assayed the passage of fluorescently-labelled dextrans of different sizes. If the nephrocyte diaphragm acts as a size-selective filter we reasoned that, like the vertebrate slit diaphragm[27], it would allow free passage of small (10,000mw) but exclude passage of large (500,000mw) dextrans (Fig. 5b). In agreement with our expectations, uptake of the 500,000mw dextran in wild-type nephrocytes is significantly lower than the 10,000mw dextran (1:3.6 n=20; Fig. 5a,f). This is likely to be an underestimation of filtration capacity because the dye:dextran molar ratio is much higher for the large (64:1) than the small (1:1) dextran. These data strongly suggest that the nephrocyte diaphragm functions as a size-based filtration diaphragm (endocytosis from foot process tips could account for low levels of large dextran uptake, Fig. 5b). We anticipated higher uptake of the large dextran in Ig-domain mutant nephrocytes because they lack diaphragms. However, while the level of uptake of the small dextran in *duf* mutant or *sns* knockdown nephrocytes is unaltered compared to wild-type, we find a dramatic reduction in uptake levels of the large dextran (Fig. 5c,d,f); uptake of large to small is 1:22.5 (n = 20) for *duf* and 1:15.3 (n = 19) for *sns*. Instead, the large dextran appears as a halo surrounding the cell (Fig. 5c,d). The thickening of basement membrane observed in *duf* nephrocytes (Fig. 3d) could explain the exclusion of the large dextran (Fig. 5e). This highlights a further parallel between nephrocytes and podocytes. An endocytosis-based clearance mechanism exists in podocytes to prevent clogging of the GBM with blood plasma proteins; the slit-

diaphragm associated protein CD2AP has been implicated in this process[24,28]. We suggest that an equivalent clearance mechanism exists in the nephrocyte and that this mechanism requires both Sns and Duf function.

Whatever the causes of reduction in filtration capability, the consequence will be disturbances to the animal's haemolymph physiology. We tested this hypothesis by feeding larvae silver nitrate, a toxin endocytosed and concentrated in nephrocytes (Fig. 5h). At low concentrations of silver nitrate, viability of control larvae is not compromised (82% eclose as adults, Fig. 5i) but *duf* larvae show a greatly reduced viability (26% eclose, Fig. 5i). A previous study showed a requirement for nephrocytes in the face of toxic stress[29]. Our data show that Ig-domain proteins are essential for this nephrocyte function.

We have highlighted similarities between podocytes and nephrocytes but there are also differences. For example, podocytes are an integral part of the nephron/renal tubule (Fig. 1a), whereas the nephrocyte is spatially separated from its renal (Malpighian) tubule (Fig. 1c). Also, the forces underlying filtration are different. In vertebrates, filtration is driven by blood pressure, whereas filtration across insect nephrocytes relies on their attachment to peristaltic tissues such as the heart and gut. These differences have contributed to the traditional view that vertebrate and invertebrate excretory systems are unrelated[1]. Nevertheless, nephron-like features are present in the excretory systems of a wide variety of invertebrates and in the protochordate *Amphioxus*, suggesting a common origin[2]. The molecular parallels between the nephrocyte and podocyte described here support this

hypothesis, and it will be of interest to determine whether nephrin/neph-like protein complexes are found in other invertebrate filtration diaphragms.

Defects in the slit diaphragm complex underlie human diseases whose unifying feature is proteinurea and kidney failure. These symptoms result in part from defective filtration, but in addition nephrin/neph1 signalling from the slit diaphragm is important for regulating podocyte behaviours such as cell survival, polarity, actin dynamics and endocytosis[30]. The relationships between the different functions of the slit diaphragm and how these in turn relate to disease pathologies are presently unclear. The fly nephrocyte also depends on the activity of a nephrin/neph1 molecular complex for survival, shape and selective endocytosis and thus provides a simple and genetically tractable model in which the multiple roles of the slit diaphragm complex can be addressed.

1. Smith, H. W. *From Fish to Philosopher* (Little, Brown, Boston, 1953).

2. Ruppert, E. E. Evolutionary Origin of the Vertebrate Nepron. *American Zoologist* **34**, 542-533 (1994).
3. Rodewald, R. & Karnovsky, M. J. Porous substructure of the glomerular slit diaphragm in the rat and mouse. *J Cell Biol* **60**, 423-33 (1974).
4. Wartiovaara, J. et al. Nephrin strands contribute to a porous slit diaphragm scaffold as revealed by electron tomography. *J Clin Invest* **114**, 1475-83 (2004).
5. Patrakka, J. et al. Congenital nephrotic syndrome (NPHS1): features resulting from different mutations in Finnish patients. *Kidney Int* **58**, 972-80 (2000).
6. Berridge, M. J. & Oschman, J. L. *Transporting Epithelia* (Academic Press, New York, 1972).
7. Crossley, A. C. in *Comprehensive Insect Physiology, Biochemistry and Pharmacology* (eds. Kerkut, G. A. & Gilbert, L. I.) 487-515 (Pergamon Press, Oxford, 1985).
8. Kowalevsky, A. Ein Beitrag zur Kenntnis der Excretions-organe. *Biol. Centralbl.* **9**, 74-79 (1889).
9. Locke, M. & Russell, V. W. in *Microscopic Anatomy of Invertebrates* (eds. Harrison, F. W. & Locke, M.) 687-709 (Wiley, 1998).
10. Kestila, M. et al. Positionally cloned gene for a novel glomerular protein--nephrin--is mutated in congenital nephrotic syndrome. *Mol Cell* **1**, 575-82 (1998).
11. Sellin, L. et al. NEPH1 defines a novel family of podocin interacting proteins. *Faseb J* **17**, 115-7 (2003).
12. Ruotsalainen, V. et al. Nephrin is specifically located at the slit diaphragm of glomerular podocytes. *Proc Natl Acad Sci U S A* **96**, 7962-7 (1999).
13. Gerke, P., Huber, T. B., Sellin, L., Benzing, T. & Walz, G. Homodimerization and heterodimerization of the glomerular podocyte proteins nephrin and NEPH1. *J Am Soc Nephrol* **14**, 918-26 (2003).
14. Barletta, G. M., Kovari, I. A., Verma, R. K., Kerjaschki, D. & Holzman, L. B. Nephrin and Neph1 co-localize at the podocyte foot process intercellular junction and form cis hetero-oligomers. *J Biol Chem* **278**, 19266-71 (2003).
15. Khoshnoodi, J. et al. Nephrin promotes cell-cell adhesion through homophilic interactions. *Am J Pathol* **163**, 2337-46 (2003).
16. Liu, G. et al. Neph1 and nephrin interaction in the slit diaphragm is an important determinant of glomerular permeability. *J Clin Invest* **112**, 209-21 (2003).
17. Donoviel, D. B. et al. Proteinuria and perinatal lethality in mice lacking NEPH1, a novel protein with homology to NEPHRIN. *Mol Cell Biol* **21**, 4829-36 (2001).
18. Tepass, U. & Hartenstein, V. The development of cellular junctions in the Drosophila embryo. *Dev Biol* **161**, 563-96 (1994).
19. Rugendorff, A., Younossi-Hartenstein, A. & Hartenstein, V. Embryonic origin and differentiation of the Drosophila heart. *Roux's Archive of Developmental Biology*, 266-280 (1994).
20. Huber, T. B. et al. The carboxyl terminus of Neph family members binds to the PDZ domain protein zonula occludens-1. *J Biol Chem* **278**, 13417-21 (2003).
21. Shih, N. Y. et al. Congenital nephrotic syndrome in mice lacking CD2-associated protein. *Science* **286**, 312-5 (1999).

22. Shih, N. Y. et al. CD2AP localizes to the slit diaphragm and binds to nephrin via a novel C-terminal domain. *Am J Pathol* **159**, 2303-8 (2001).
23. Boute, N. et al. NPHS2, encoding the glomerular protein podocin, is mutated in autosomal recessive steroid-resistant nephrotic syndrome. *Nat Genet* **24**, 349-54 (2000).
24. Kim, J. M. et al. CD2-associated protein haploinsufficiency is linked to glomerular disease susceptibility. *Science* **300**, 1298-300 (2003).
25. Schwarz, K. et al. Podocin, a raft-associated component of the glomerular slit diaphragm, interacts with CD2AP and nephrin. *J Clin Invest* **108**, 1621-9 (2001).
26. Galletta, B. J., Chakravarti, M., Banerjee, R. & Abmayr, S. M. SNS: Adhesive properties, localization requirements and ectodomain dependence in S2 cells and embryonic myoblasts. *Mech Dev* **121**, 1455-68 (2004).
27. Kramer-Zucker, A. G., Wiessner, S., Jensen, A. M. & Drummond, I. A. Organization of the pronephric filtration apparatus in zebrafish requires Nephrin, Podocin and the FERM domain protein Mosaic eyes. *Dev Biol* **285**, 316-29 (2005).
28. Akilesh, S. et al. Podocytes use FcRn to clear IgG from the glomerular basement membrane. *Proc Natl Acad Sci U S A* **105**, 967-72 (2008).
29. Das, D., Aradhya, R., Ashoka, D. & Inamdar, M. Post-embryonic pericardial cells of Drosophila are required for overcoming toxic stress but not for cardiac function or adult development. *Cell Tissue Res* **331**, 565-70 (2008).
30. Huber, T. B. & Benzing, T. The slit diaphragm: a signaling platform to regulate podocyte function. *Curr Opin Nephrol Hypertens* **14**, 211-6 (2005).

Acknowlegements. Felix Evers, Zoltan Cseresnyes and M. Guerra for technical assistance. Susan Abmayr, Lynn Cooley, Chris Doe, Markus Affolter, Karl Fischbach and Karl Tryggvason for reagents. We thank Maneesha Inamdar, Adrian Woolf and members of the Skaer lab for helpful discussions and Elisabeth Knust and Wieland B. Huttner for their generous support. This work was supported by Wellcome Trust grants awarded to H.S. (072441 and 079221, H.W., B.D., H.S.); Deutsche Forschungsgemeinschaft (SFB 590) awarded to Elisabeth Knust (F.G.), ARC 1242 (H.W., B.D., H.S., F.G.); MEC grant awarded to M.R-G. (BFU2007-62201, S.P-S., M.R-G.); Fundación Ramón Areces grant to the CBMSO (M.R-G.); EC grant LSHG-CT-2004-511978 to MYORES (M.R-G.); an FPU fellowship from the MEC awarded to A.G-L.

Author contribution

B.D., H.S., M.R-G. designed and directed the project. B.D., H.W., M.R-G. and S.P-S. performed the experiments. F.G. and M.W-B. provided invaluable technical assistance. A.G-L. and R.A. provided materials. B.D. and H.S. wrote the paper. All authors discussed results and commented on the manuscript.

Figure 1 | The anatomy of the nephrocyte filtration barrier is very similar to the glomerular filtration barrier.

a-d, Schematic drawings of the vertebrate nephron (a), glomerular filtration barrier (b), insect excretory system (c), and nephrocyte filtration barrier (d). Red and black arrows indicate ultrafiltration and direction of filtrate flow respectively, asterisk indicates urinary space (b) or extracellular lacunae (d). e,f, Two classes of *Drosophila* nephrocyte (arrowheads), garland nephrocytes stained with anti-HRP (e) and pericardial nephrocytes stained with anti-Pericardin (f). Higher magnification images are shown in e^{i} and f^{i}. g-i, Transmission electronmicrographs of stage 16 embryonic garland nephrocytes. g, A cluster of four nephrocytes surrounding the proventiculus (pv) are indicated with numbers, connective fibres with arrowhead. h and i, Higher magnification of a garland nephrocyte cell surface (h) and nephrocyte diaphragm (i). Arrowheads indicate nephrocyte diaphragm, asterisk indicates extracellular lacunae. Scale bars 2µm (g), 100nm (h,i). fp, foot process; sd, slit diaphragm; nd, nephrocyte diaphragm; bm, basement membrane.

Figure 2 | Sns and Duf are expressed in *Drosophila* nephrocytes.

a-g, Sns (a,d,f) and Duf (b,c,e,g) expression in garland (a,b,d,e) and pericardial (c,f,g) nephrocytes. Stage 16 embryos (a,b, arrowheads), first instar larva (c, green, arrowheads), and third instar larvae (d-g, green). The actin cytoskeleton has been counterstained with AlexaFluor568 phalloidin in c,d,f,g. h, Sns and Duf co-localise. anti-Sns (h, green), anti-Duf (h^{i}, red) and merged image (h^{ii}, yellow).

Antibodies directed against each of the proteins were used in each case except for b and c in which a *duf*-nuclear *lacZ* reporter was used (*rP298*). i-l, Clusters of approximately 6-8 wild-type (i,k), *sns* (j) or duf,rst (l) embryonic garland cells stained with anti-Duf (i,j) or anti-Sns (k,l) . m-p, wild-type (m,o), *sns-RNAi* (n) and *Df(1)duf*$^{sps\text{-}1}$ (p) third instar garland cells stained for anti-Duf and anti-Sns (red and green respectively, merge appears yellow) and TO-PRO-3 for DNA (blue). Single optical section (m,n) or *z*-projection of stack from cell surface (o,p) are shown. q-u, Electron micrograph of wild-type third instar garland cells immunogold-stained for anti-Sns (q), anti-Duf (r,s) or double labelled with anti-Sns and anti-Duf (t,u). For single labelling 10nm gold particles are used and for double labelling 5nm (arrowhead) and 10nm (arrow) gold particles are used to recognise Sns and Duf respectively. Scale bars 100nm (q-t) and 10nm (u).

Figure 3 | Sns and Duf are required for nephrocyte diaphragm formation and normal morphology.

a,b, *sns* (a, a^{i}) and *duf,rst* (b) embryonic garland cells lack nephrocyte diaphragms and lacunae but have patches of electron-dense subcortical material (a, arrowheads). a^{i}, higher magnification of a. Occasional, small lacunae are found (asterisk) but these lack nephrocyte diaphragms (b, arrowhead). c,d, Wild-type (c) and *duf* (d) third instar garland cells. c, nephrocyte diaphragms (arrowheads) and associated lacunae (asterisk) densely populate the nephrocyte surface. d, *duf* nephrocytes have occasional, small lacunae (arrowheads), but lack nephrocyte diaphragms and have a substantially thickened basement

membrane (bm), having an average thickness of 202nm but reaching a depth of up to 315nm in some regions. e,f, Scanning electron micrographs of wild-type (e) and *duf* (f) third instar garland nephrocytes stripped of overlying basement membrane by collagenase treatment. *duf* nephrocytes lack the furrows corresponding to diaphragm rows. g,h, Wild-type (g) and *duf* (h) Viking-GFP (collagen IV) third instar garland cells, stained with anti-GFP (green). Significantly more Viking is deposited around *duf* nephrocytes compared with wild-type (arrowheads and inset). In addition, the number of garland cells is reduced in *duf* larvae compared with wild-type, suggesting that mutant cells ultimately die. i,j, Overexpression of *sns* (i) or human nephrin (j) in embryonic garland cells. Morphology of the nephrocyte diaphragms and foot processes are abnormal (arrowheads). Scale bars 200nm (a,c,d), 100nm (a^{i},b), 50nm (i-j), 5µm (e,f). os, oesophagus, pv, proventriculus, tr, trachea.

Figure 4 | Analysis of slit diaphragm-associated protein orthologues in the fly nephrocyte.

a-f, Third instar garland (a,c,e) and pericardial (b,d,f) nephrocytes hybridised with probes directed against *Mec2* (a stomatin domain containing protein with similarity to NPHS2/podocin) (a,b), *pyd* (c,d) and *CG31012* (e,f). g, Pyd and Duf co-localise. Pyd-GFP third instar garland nephrocytes stained for GFP (g, green), anti-Duf (g^{i}, red) and merged image (g^{ii}, yellow). h, Schematic drawing of known protein interactions between the major components of the vertebrate slit diaphragm (black arrows) and nephrocyte diaphragm (described here and

elsewhere, red arrows). i, Schematic drawing of the *Drosophila* orthologues of slit diaphragm-associated proteins showing conserved domains: PDZ-binding domain (THV), PDZ domain (PDZ), stomatin domain (STO) and SH3 domain (SH3). Region of the protein used in the yeast two-hybrid analysis is outlined in red, single lines represent transmembrane domains. The entire extracellular domains of Sns and Duf are not shown. j, Yeast two-hybrid analysis of interactions between Sns or Duf and Pyd, CG31012, Mec2 and negative control (empty vector). Direct protein interaction is indicated by growth of yeast colonies on selective media (H- 5mM 3'AT). k, Co-immunoprecipitation experiments in transiently transfected S2 cells, showing a physical interaction between Duf and Pyd-V5. The asterisk indicates a cleaved form of Duf that is also coimmunoprecipitated with Pyd. Unlabelled arrowhead on left corresponds to Pyd. l, Schematic drawing of molecular interactions at the nephrocyte diaphragm. Sns (green), Duf (black), Mec2 (yellow), Pyd (blue), CG31012 (red), red arrow indicates direction of filtration and asterisk extracellular lacuna. Putative links to the actin cytoskeleton or to intracellular signalling based on analogy with the equivalent protein complex at the slit diaphragm are shown. bm, basement membrane.

Figure 5 | Sns and Duf are required for nephrocyte filtration

a,c,d, Third instar larval garland nephrocytes from wild-type (a), *duf* (c) and *sns RNAi* knockdown (d) animals co-incubated with 10,000mw (magenta) and 500,000mw (green) fluorescently-labelled dextran. Transmitted light, 10,000mw,

500,000mw and merged images are shown. Inset in c,d shows merged image of transmitted light and 500,000mw channels. b,e, Schematic drawing of filtration and endocytosis in wildtype (b) and *sns* or *duf* mutant (e) nephrocytes. f, Quantification of dextran uptake for the small (magenta) and large (green) dextrans in wild-type, *duf* and *sns RNAi* knockdown garland cells. Y axis corresponds pixels number above background threshold (error bars, S.E.M). g, control nephrocyte incubated with dextran at 4^{o}C showing no dextran uptake (g^{i}). h, 10µm section of two wild-type garland nephrocytes from a larva fed with $AgNO_3$. $AgNO_3$ concentrates within the nephrocyte (brown). i, Percentage of eclosing sibling control or *duf* adults fed yeast paste (grey) or yeast paste laced with $AgNO_3$ (blue) (n = 65, 68, 55 and 57). bm, basement membrane.

Supplementary Figure 1 | Sns and Duf co-localise in embryonic nephrocytes. a-c, Wild-type stage 11 (a),14 (b) and 16 (c) embryos stained with anti-Duf (green) and anti-Sns (red). Higher magnification images are shown in a^{i}-c^{i}, white arrows indicate garland cells. Sns and Duf accumulate at points of contact between garland nephrocytes during stages 11 and 14 and resolve into a filigree pattern by stage 16.

Supplementary Figure 2 | Phenotypic analysis of *sns* and *duf* mutants. a-c, Stage 16 embryos stained for anti-Pericardin (red) to visualize pericardial nephrocytes. a, Heterozygous control embryo stained for *wg-Lac*Z balancer chromosome (green). b,c, pericardial nephrocytes are specified correctly and

have wild-type gross anatomy in *rst, duf* double (b) and *sns* (c) mutant embryos. Higher magnification images are shown in a^i-c^i. d-f, Stage 16 embryos stained for anti-HRP (red) to visualize garland nephrocytes. d, Heterozygous control embryo stained for *wg-Lac*Z balancer chromosome (green). e,f, garland nephrocytes are specified correctly and have wild-type gross anatomy in *rst, duf* double (e) and *sns* (f) mutant embryos. Higher magnification images are shown in d^i-f^i. g-k, *sns* and *duf* garland cells are binucleate as in wild-type. g-i, Electron micrographs of wild-type (g) *sns* (h) and rst, *duf* (i) embryonic garland nephrocytes (nuclei are indicated by red asterisks). j,k, Third instar garland nephrocytes from sibling control (j) and *duf* (k) larvae stained for actin (green) and DNA (blue). l-n, Electron micrographs of wild-type (l) and *sns* (m,n) stage 14 embryonic garland cells. l, Nephrocyte diaphragms and associated lacunae (arrowheads) develop in the gap between two closely apposed garland cells (asterisk). m,n, Nephrocyte diaphragms never develop in *sns* garland cells and lacunae are found only very infrequently (n, arrowhead). Arrows indicate closely associated garland cells (l,m). o, *duf* larvae were scored by PCR-genotyping carcasses remaining after dissection of nephrocytes[31]. *rst*-specific primers (positive control - lanes 1 and 3) and *duf*-specific primers (lanes 2 and 4) from *duf* (lanes 1 and 2) and sibling control (lanes 3 and 4) larvae. Scale bars 1μm (g-l), 500nm (l,m), 100nm (n).

Supplementary Figure 3 | Viking deposition is greater in *duf* nephrocytes

a, b, Pixel intensity profiles for Viking-GFP (collagen IV) (a) and F-actin (b). A 100 pixel-long line (~10μm) was drawn bisecting the cell periphery (labelled white

line in inset) and intensity profiles were measured using image-J software. Peak fluorescence of Viking (a) in *duf* nephrocytes (red, n = 30) is wider than wild-type (blue, n = 7), whereas the peak fluorescence of a control staining (F-actin) is the same (b).

Supplementary Figure 4 | Amino acid sequence comparison between *Drosophila* Mec2 and human podocin

Sequences were aligned using VectorNTIExplorer, identical residues are indicated in yellow, similar residues in green, transmembrane domain (tm) and stomatin signature sequence (stomatin) are underlined.

METHODS SUMMARY

Fly strains

Flies were reared on standard food at room temperature, 18^{o}C or 25^{o}C. The strains used are listed in the Methods.

Nephrocyte filtration assay

Garland cells were dissected, incubated with AlexaFluor568-Dextran (10,000mw) and Fluorescein-Dextran (500,000mw) (Molecular probes) at a concentration of 0.33mg/ml at 25^{o}C for 5 minutes, washed on ice, fixed and mounted. Dextran uptake was quantified by counting pixel number exceeding background threshold using Volocity software.

Toxin stress assay

First instar flies of the appropriate genotype were transferred to agar-only plates supplemented with yeast paste or with yeast paste containing $AgNO_3$ (2g yeast in 3.5ml of 0.003% $AgNO_3$), and allowed to develop at 25^{o}C. Percentage of eclosing adults was scored.

Antibodies

Antibodies used were: anti-Sns (1:200, S.Abmayr), anti-Kirre (1:200, K. Fischbach), anti-Duf extracellular (1:50, M.R-G.), anti-βgal (1:1000, ICN Biomedicals), anti-HRP (1:200, Jackson ImmunoResearch), anti-Pericardin (1:2, DSHB), anti-GFP (1:500, Invitrogen Molecular probes).

Confocal and electron microscopy

Confocal and electron microscopy was carried out using standard techniques. For immuno-electron microscopy, dissected larval garland cells were fixed in 4% formaldehyde + 0.05% glutaraldehyde, embedded in gelatin, cryosectioned and incubated

with anti-Duf extracellular (1:5), anti-Kirre (1:20), or anti-Sns (1:20) followed by 5nm and 10nm gold-conjugated secondary antibody.

Yeast two-hybrid

The intracellular domains of Sns and Duf were tested for interaction with: Pyd (isoform f); CD2AP (SD08724); C-terminal cytoplasmic domain of Mec2 using the Clontech Matchmaker GAL4 two-hybrid system. Interaction was indicated by growth in absence of histidine. 5mM 3'AT (Sigma) was included to titrate residual auto-activation from the bait fusion proteins.

Co-immunoprecipitation experiments

Drosophila S2 cells transiently co-transfected with pMK33/pMtHy-duf and pAC5.1V5-His-pyd were induced for 20 hours with 0.7mM $CuSO_4$. Total cell lysate was split and each half immunoprecipitated with either anti-V5 or anti-Kirre and probed with anti-Kirre and anti-V5 following standard protocols.

METHODS

Fly strains. The following fly genotypes were used: OregonR (wild-type strain); *sns*^{XB3} and *UAS-sns* (gift from S. Abmayr); for embryonic analysis of *duf Df(1)w*^{67k30} hemizygotes were used; for larval analysis of *duf Df(1)w*^{67k30}*/Df(1)N*^{5419} transheterozygous or *Df(1)duf*$^{sps-1}$ [small deficiency removing the *duf* locus only, a description of this allele will published elsewhere (Prieto-Sánchez et al., in preparation)] were used; *rP298* (*duf-LacZ*); *UAS-Pyd-GFP* (gift from M. Affolter); *Viking-GFP* (gift from L.Cooley); *UAS-sns-RNAi* (a 1047bp fragment was obtained by PCR from *sns* cDNA using primers 5'-CCAGTTCGTATAATGACACCG and 5'-CCTACAGCTATACGAGGTGTC and used to make intron-spliced hairpin RNA according to[31]; *UAS-nephrin* [human NPHS1 cDNA (gift from K. Tryggvason) cloned into pUAST]; *G447.2-GAL4* (embryonic garland cell driver; gift from R. Reuter); *Prospero-Gal4* (larval garland cell driver; gift from Chris Doe). Fly crosses were maintained at 25^{o}C except for the overexpression experiment when animals were maintained at 29^{o}C to ensure maximum transgene expression. Marked balancer chromosomes (Kr-Gal4, UAS-GFP) and/or PCR-genotyping[32] from carcasses remaining after dissection were used to identify appropriate genotypes.

Nephrocyte filtration assay. Garland nephrocytes (including a small portion of oesophagus and the proventriculus) were dissected from third instar larvae in Shields and Sang medium (Sigma), then transferred to media containing AlexaFluor568-Dextran (10,000mw) and Fluorescein-Dextran (500,000mw) (Molecular probes) at a concentration of 0.33mg/ml and incubated at 25^{o}C for 5 minutes. The cells were washed on ice for 10 minutes in cold PBS, fixed in 4% formaldehyde for 10 minutes at room

temperature, rinsed once in PBS and then mounted in vectashield (Vectorlabs). All post-dissection procedures were carried out in the dark. A single confocal section of the cell midpoint was taken using a Leica SP1 confocal microscope and dextran uptake was quantified by counting pixel number exceeding background threshold within the sample area (typically the whole cell) using Volocity software. Average fluorescence from the proventriculus epithelium (where dextran uptake does not occur) was used to set the background threshold. The same threshold was used for all experiments. Control cells incubated with Dextran on ice showed no uptake.

Toxin stress assay: Flies of the appropriate genotype were allowed to lay on standard apple juice plates supplemented with yeast. After approximately 24 hours, freshly emerging first instar larvae from this plate were transferred to agar-only plates supplemented with yeast paste or with yeast paste containing $AgNO_3$ (2g yeast in 3.5ml of 0.003% $AgNO_3$), and allowed to develop at 25^{o}C. Percentage of eclosing adults was scored.

In situ hybridisation and immunohistochemistry. Whole mount in situ hybridization and immunohistochemistry to embryos and third instar nephrocytes were carried out using standard techniques. Antibodies used: anti-Sns (1:200, gift from S. Abmayr), anti-Kirre (1:200, gift from K. Fischbach), anti-Duf extracellular [the generation of anti-Duf extracellular antisera will be published elsewhere (1:50, Prieto-Sánchez et al., in preparation), anti-βgal (1:1000, ICN Biomedicals), anti-HRP (1:200, Jackson ImmunoResearch), anti-Pericardin (1:2, DSHB), anti-GFP (1:500, Invitrogen Molecular probes), AlexaFluor 488 phalloidin and AlexaFluor 568 phalloidin (1:20, Invitrogen Molecular probes), TOTO3 and TO-PRO-3 (1:100, Invitrogen Molecular probes).

Confocal and electron microscopy. Confocal and electron microscopy were carried out using standard techniques. For immuno-electron microscopy, dissected garland cells were fixed in 4% formaldehyde + 0.05% glutaraldehyde, embedded in gelatin, cryosectioned and incubated with anti-Duf extracellular (1:5), anti-Kirre (1:20), or anti-Sns (1:20) followed by 5nm and10nm gold-conjugated secondary antibody. In some cases confocal images correspond to *z*-projections from a series of confocal sections.

Yeast two-hybrid. The intracellular domains of Sns and Duf were used as bait (cloned into pGBKT7, Clontech) and tested for interaction with: Pyd (isoform f); CD2AP (SD08724); C-terminal cytoplasmic domain of Mec2 (all cloned into pGADT7, Clontech). Interaction was indicated by growth in absence of histidine. 5mM 3'AT (Sigma) was included to titrate residual auto-activation from the bait fusion proteins.

Co-immunoprecipitation experiments. *Drosophila* S2 cells transiently co-transfected with pMK33/pMtHy-duf and pAC5.1V5-His-pyd were induced for 20 hours with 0.7mM $CuSO_4$. Total cell lysate was split and each half immunoprecipitated with either anti-V5 or anti-Duf and probed consecutively with anti-Duf and anti-V5 or anti-V5 and anti-Duf, respectively, following standard protocols.

31 Nagel, A. C., Maier, D. & Preiss, A. Green fluorescent protein as a convenient and versatile marker for studies on functional genomics in Drosophila. *Dev Genes Evol* **212**, 93-8 (2002).

32 Strunkelnberg, M. et al. rst and its paralogue kirre act redundantly during embryonic muscle development in Drosophila. *Development* **128**, 4229-39 (2001).

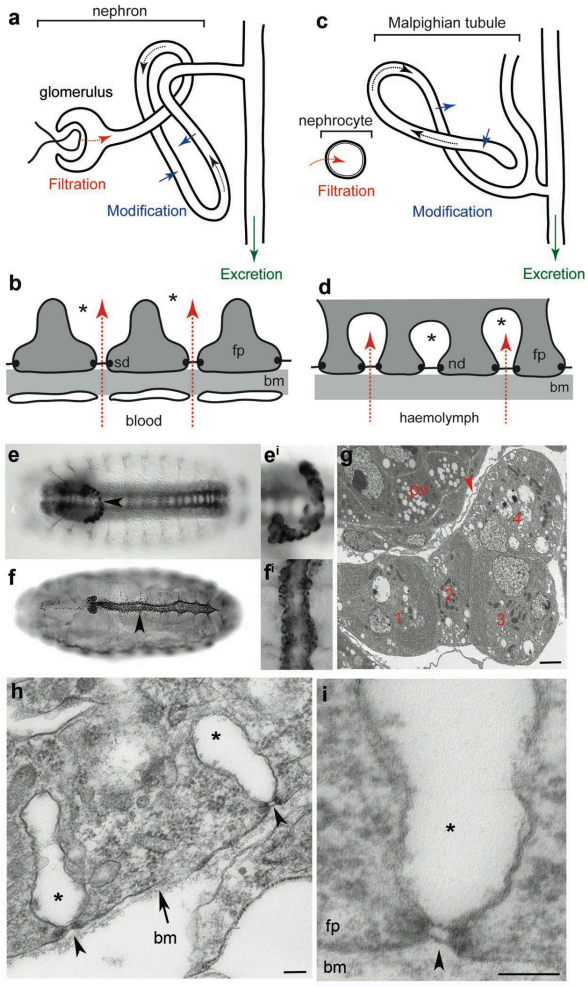
a
nephron
glomerulus
Filtration
Modification
Excretion
c
Malpighian tubule
nephrocyte
Filtration
Modification
Excretion
b
sd
fp
bm
blood
d
nd
fp
bm
haemolymph
e
e'
f
f'
g
DV
4
2
1
3
h
bm
i
fp
bm

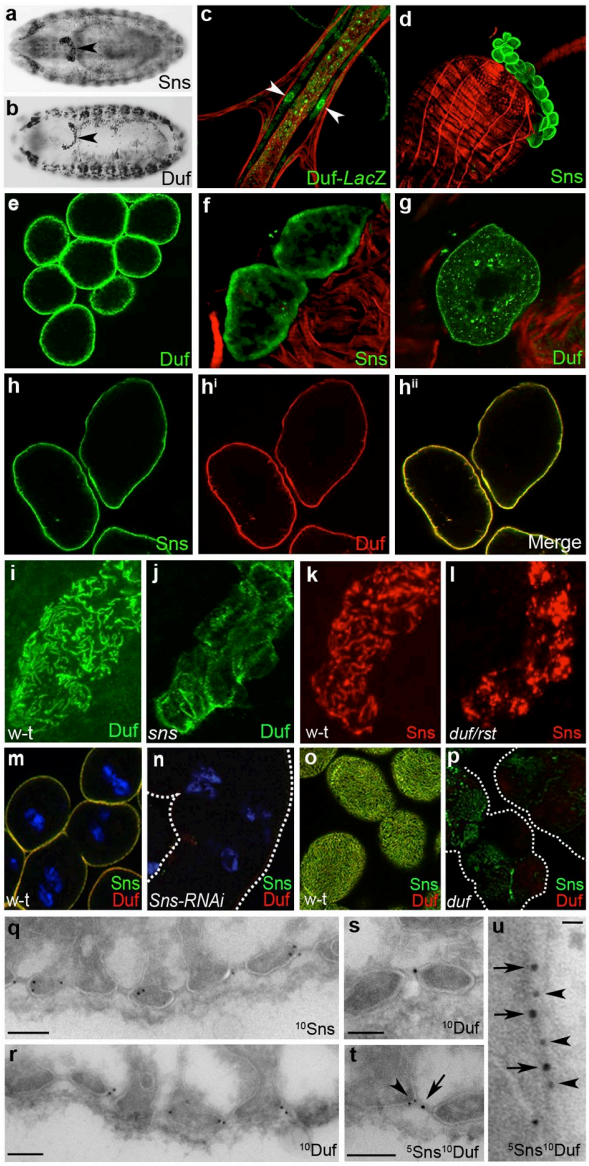
a
Sns
b
Duf
c
Duf-LacZ
d
Sns
e
Duf
f
Sns
g
Duf
h
Sns
hi
Duf
hii
Merge
i
w-t
Duf
j
sns
Duf
k
w-t
Sns
l
duf/rst
Sns
m
w-t
Sns
Duf
n
Sns-RNAi
Sns
Duf
o
w-t
Sns
Duf
p
duf
Sns
Duf
q
10Sns
s
10Duf
u
r
10Duf
t
5Sns10Duf
5Sns10Duf

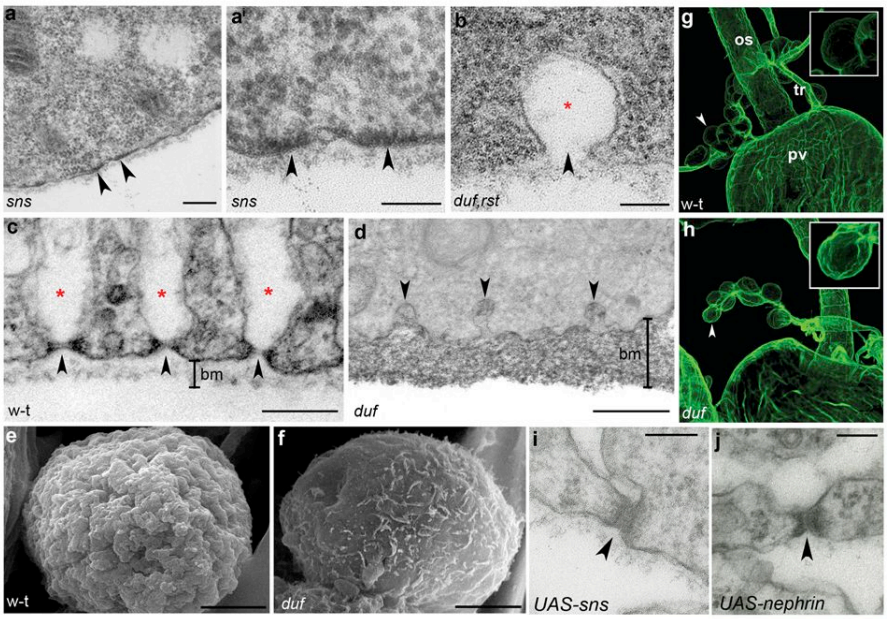
a
sns
a'
sns
b
duf,rst
g
os
tr
pv
w-t
c
bm
w-t
d
bm
duf
h
duf
e
w-t
f
duf
i
UAS-sns
j
UAS-nephrin

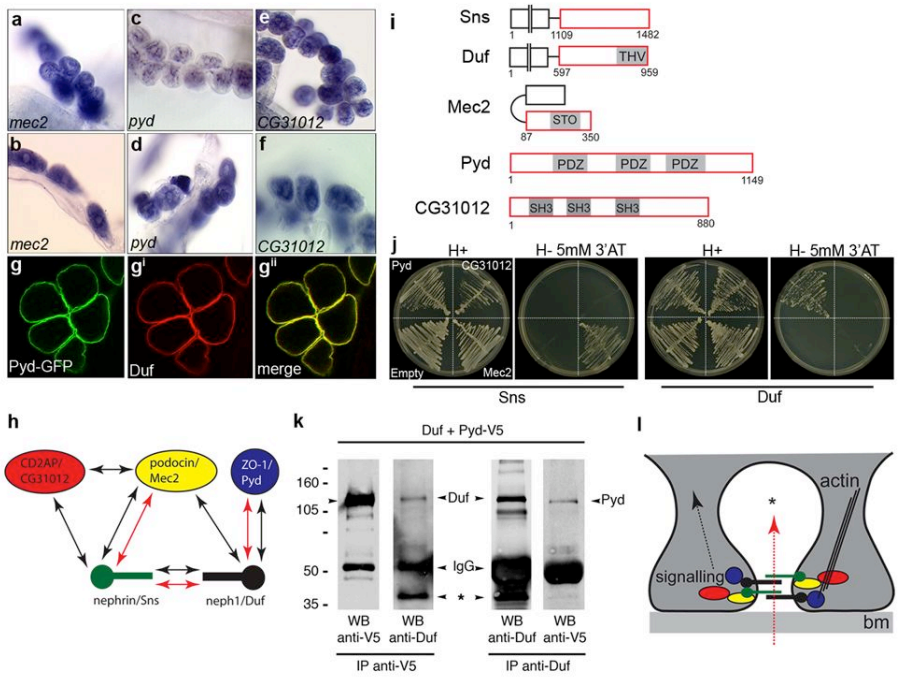
a
mec2
c
pyd
e
CG31012
b
mec2
d
pyd
f
CG31012
g
Pyd-GFP
gI
Duf
gII
merge
i
Sns
1
1109
1482
Duf
THV
1
597
959
Mec2
STO
87
350
Pyd
PDZ
PDZ
PDZ
1
1149
CG31012
SH3
SH3
SH3
1
880
j
H+
H- 5mM 3'AT
H+
H- 5mM 3'AT
Pyd
CG31012
Empty
Mec2
Sns
Duf
h
CD2AP/
CG31012
podocin/
Mec2
ZO-1/
Pyd
nephrin/Sns
neph1/Duf
k
Duf + Pyd-V5
160
105
50
35
Duf
IgG
*
Pyd
WB
anti-V5
WB
anti-Duf
WB
anti-Duf
WB
anti-V5
IP anti-V5
IP anti-Duf
l
actin
*
signalling
bm

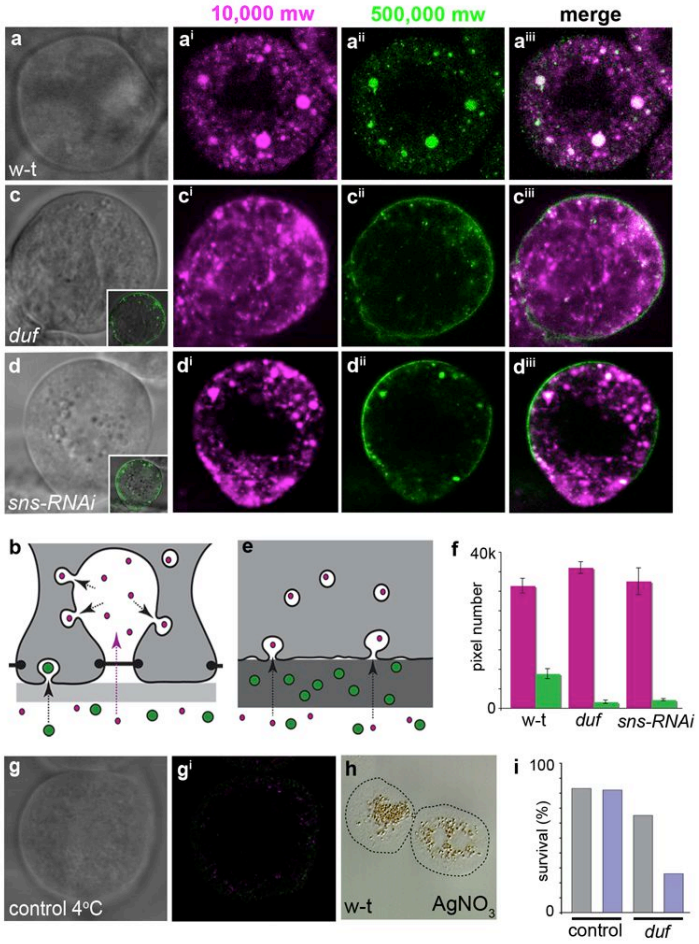
10,000 mw
500,000 mw
merge
a
a^i
a^ii
a^iii
w-t
c
c^i
c^ii
c^iii
duf
d
d^i
d^ii
d^iii
sns-RNAi
b
e
f
40k
pixel number
0
w-t
duf
sns-RNAi
g
g^i
control 4°C
h
w-t
AgNO3
i
100
survival (%)
0
control
duf

Supplementary Table 1 | Components of the slit diaphragm and their fly orthologues

Human gene/protein	Disease/phenotype	Fly orthologues
NPHS1/nephrin	Congenital nephrotic syndrome of the Finnish type	*sticks and stones*[1] *hibris*[2]
neph1	Experimental congenital nephrotic syndrome	*dumbfounded* (*kirre*)[3] *roughest* (*irregular chiasm-C*)[4]
NPHS2/podocin	Experimental congenital nephrotic syndrome	*Mec2*[*]
CD2AP	Sporadic and inherited nephrotic syndromes	*CG31012*[5]
ZO-1	Not known	*polychaetoid*[6]

* There are seven stomatin domain-containing proteins in *Drosophila* with similarity to podocin. Mec2 is the only one expressed in nephrocytes (data not shown).

1 Bour, B. A., Chakravarti, M., West, J. M. & Abmayr, S. M. Drosophila SNS, a member of the immunoglobulin superfamily that is essential for myoblast fusion. *Genes Dev* **14**, 1498-511 (2000).

2 Artero, R. D., Castanon, I. & Baylies, M. K. The immunoglobulin-like protein Hibris functions as a dose-dependent regulator of myoblast fusion and is differentially controlled by Ras and Notch signaling. *Development* **128**, 4251-64 (2001).

3 Ruiz-Gomez, M., Coutts, N., Price, A., Taylor, M. V. & Bate, M. Drosophila dumbfounded: a myoblast attractant essential for fusion. *Cell* **102**, 189-98 (2000).

4 Strunkelnberg, M. et al. rst and its paralogue kirre act redundantly during embryonic muscle development in Drosophila. *Development* **128**, 4229-39 (2001).

5 Johnson, R. I., Seppa, M. J. & Cagan, R. L. The Drosophila CD2AP/CIN85 orthologue Cindr regulates junctions and cytoskeleton dynamics during tissue patterning. *J Cell Biol* **180**, 1191-204 (2008).

6 Takahisa, M. et al. The Drosophila tamou gene, a component of the activating pathway of extramacrochaetae expression, encodes a protein homologous to mammalian cell-cell junction-associated protein ZO-1. *Genes Dev* **10**, 1783-95 (1996).

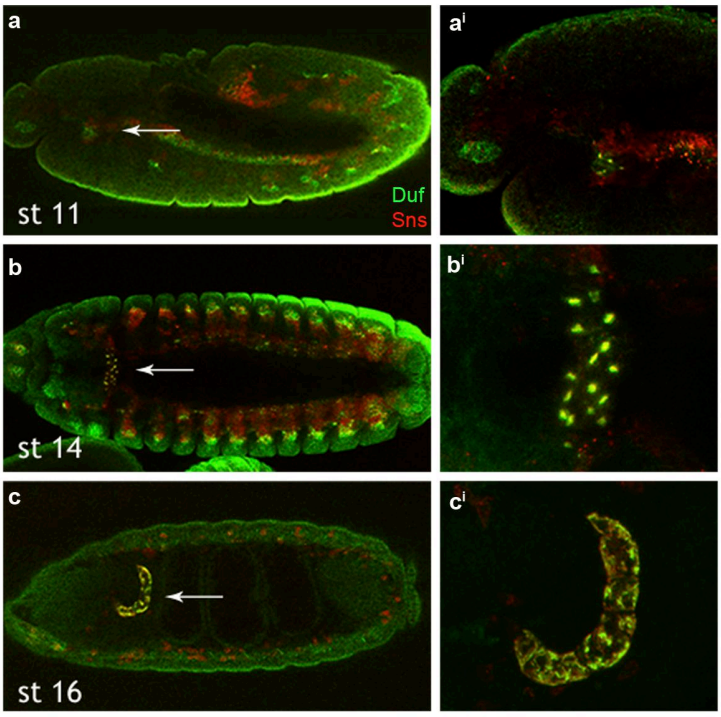
a
st 11
Duf
Sns
a^i
b
st 14
b^i
c
st 16
c^i

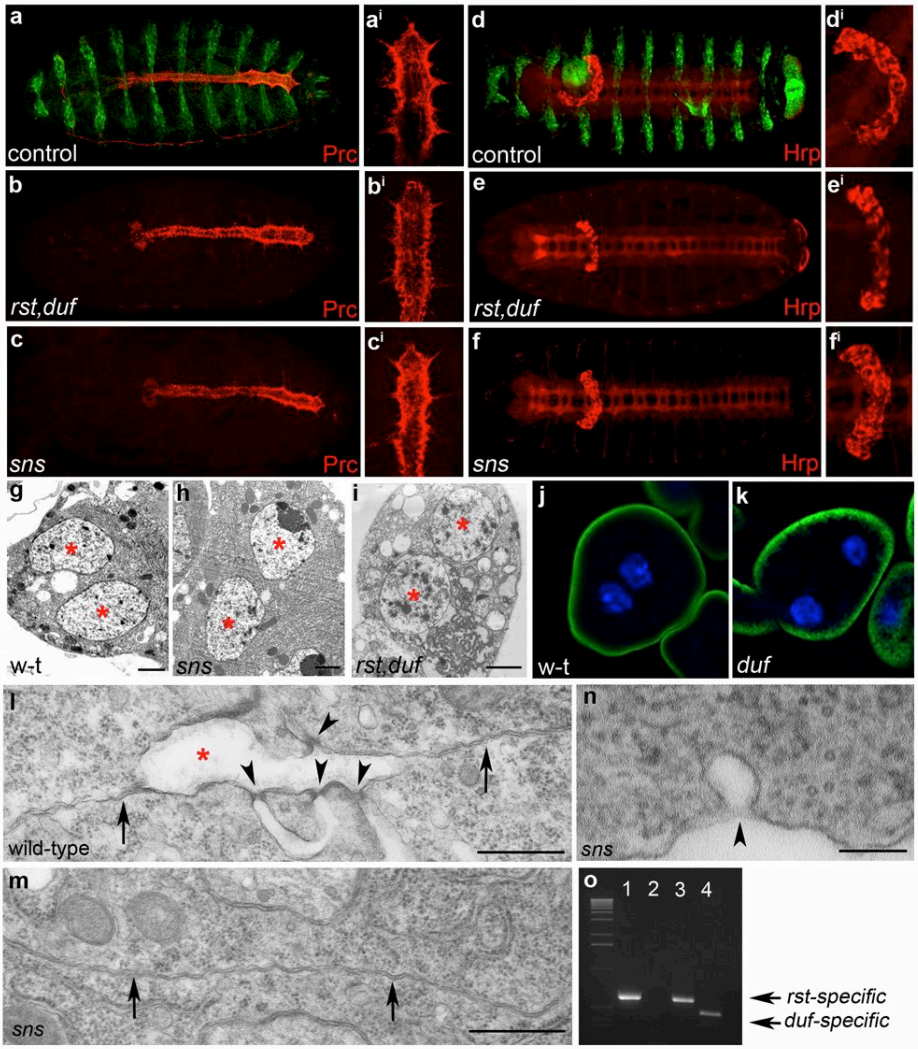
a
control
Prc
a^i
d
control
Hrp
d^i
b
rst,duf
Prc
b^i
e
rst,duf
Hrp
e^i
c
sns
Prc
c^i
f
sns
Hrp
f^i
g
w-t
h
sns
i
rst,duf
j
w-t
k
duf
l
wild-type
n
sns
m
sns
o
1 2 3 4
rst-specific
duf-specific

a

Viking-GFP (Collagen IV)

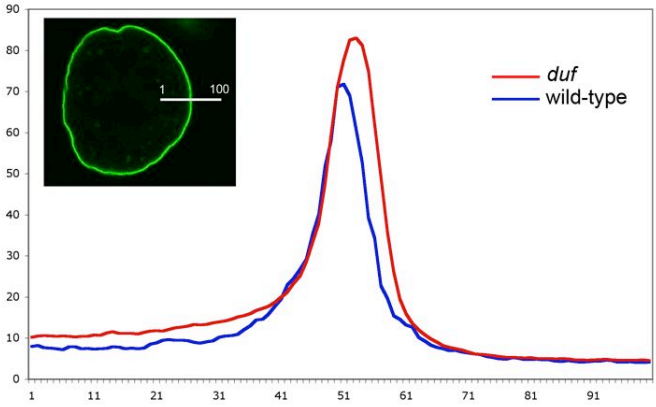

b

F-Actin

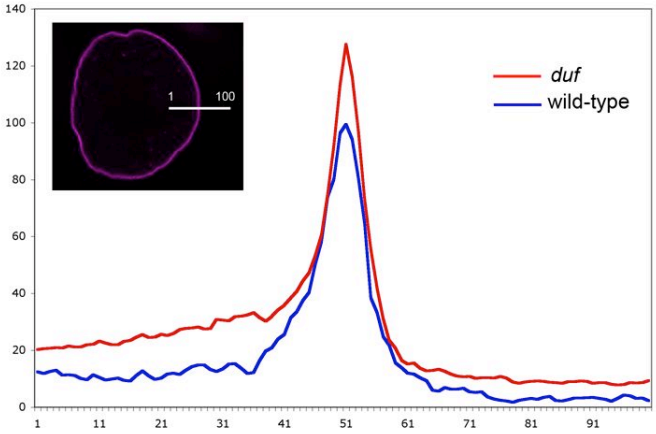

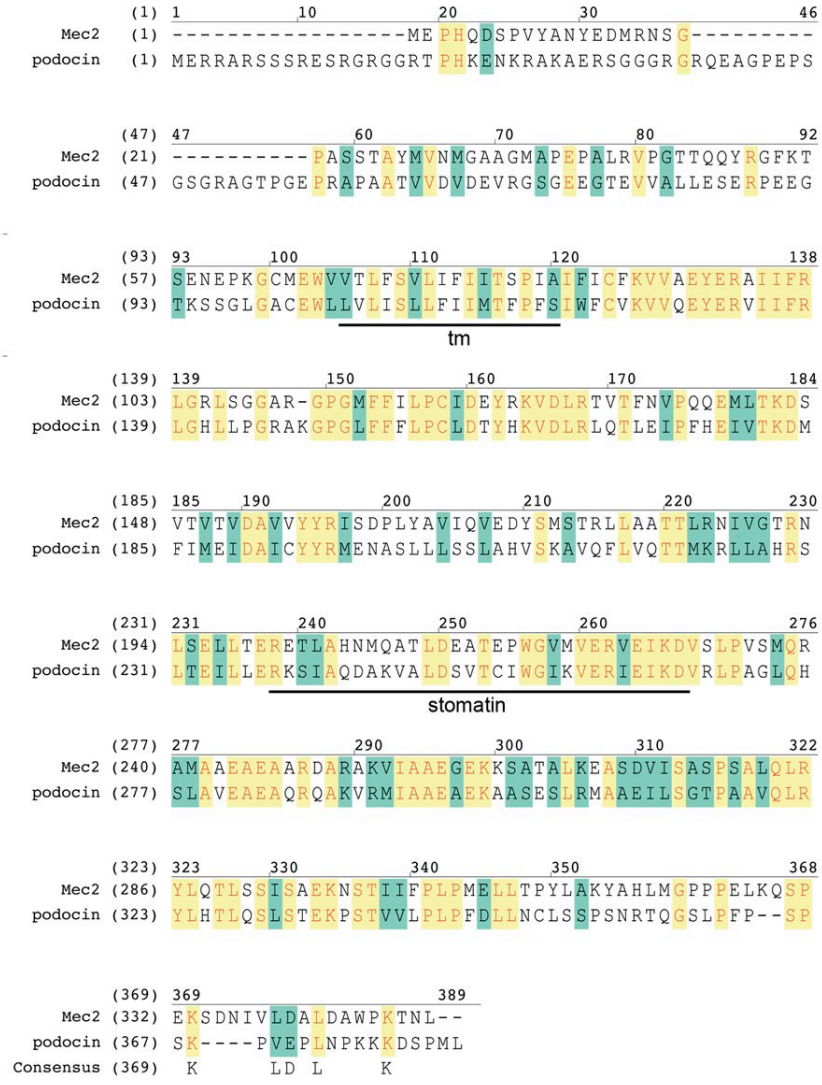
(1) 1 10 20 30 46
Mec2 (1) ----------ME PHQDSPVYANYEDMRNSG---------
podocin (1) MERRARSSSRESRGRGGRT PHKENKRAKAERSGGGRGRQEAGPEPS
(47) 47 60 70 80 92
Mec2 (21) ----------PASSTAYMVNMGAAGMAPEPALRVPGTTQQYRGFKT
podocin (47) GSGRAGTPGEPRAPAATVVDVDEVRGSGEEGTEVVALLESERPEEG
(93) 93 100 110 120 138
Mec2 (57) SENEPKGCMEWVVTLFSVLIFIITSPIAIFICFKVVAEYERAIIFR
podocin (93) TKSSGLGACEWLLVLISLLFIIMTFPFSIWFCVKVVQEYERVIIFR
tm
(139) 139 150 160 170 184
Mec2 (103) LGRLSGGAR-GPGMFFILPCIDEYRKVDLRTVTFNVPQQEMLTKDS
podocin (139) LGHLLPGRAKGPGLFFFLPCLDTYHKVDLRLQTLEIPFHEIVTKDM
(185) 185 190 200 210 220 230
Mec2 (148) VTVTVDAVVYYRISDPLYAVIQVEDYSMSTRLLAATTLRNIVGTRN
podocin (185) FIMEIDAICYYRMENASLLLSSLAHVSKAVQFLVQTTMKRLLAHRS
(231) 231 240 250 260 276
Mec2 (194) LSELLTERETLAHNMQATLDEATEPWGVMVERVEIKDVSLPVSMQR
podocin (231) LTEILLERKSIAQDAKVALDSVTCIWGIKVERIEIKDVRLPAGLQH
stomatin
(277) 277 290 300 310 322
Mec2 (240) AMAAEAEAARDARAKVIAAEGEKKSATALKEASDVISASPSALQLR
podocin (277) SLAVEAEAQRQAKVRMIAAEAEKAASESLRMAAEILSGTPAAVQLR
(323) 323 330 340 350 368
Mec2 (286) YLQTLSSISAEKNSTIIFPLPMELLTPYLAKYAHLMGPPPELKQSP
podocin (323) YLHTLQSLSTEKPSTVVLPLPFDLLNCLSSPSNRTQGSLPFP--SP
(369) 369 389
Mec2 (332) EKSDNIVLDALDAWPKTNL--
podocin (367) SK----PVEPLNPKKKDSPML
Consensus (369) K LD L K